

Water Resources Research

RESEARCH ARTICLE

10.1002/2016WR019887

Special Section:

Disturbance Hydrology

Key Points:

- A snow aridity index explained 11% more of the baseline NDVI variability than the snow water equivalent
- Bark beetle disturbance can supersede moisture stress to vegetation productivity given sufficient forest mortality
- Postdisturbance forested landscapes may be more sensitive to snowrelated drought

Correspondence to:

J. F. Knowles, John.Knowles@Colorado.edu

Citation:

Knowles, J. F., L. R. Lestak, and N. P. Molotch (2017), On the use of a snow aridity index to predict remotely sensed forest productivity in the presence of bark beetle disturbance, *Water Resour. Res.*, *53*, 4891–4906, doi:10.1002/2016WR019887.

Received 4 OCT 2016 Accepted 22 MAY 2017 Accepted article online 26 MAY 2017 Published online 15 JUN 2017

On the use of a snow aridity index to predict remotely sensed forest productivity in the presence of bark beetle disturbance

John F. Knowles¹, Leanne R. Lestak¹, and Noah P. Molotch^{1,2,3}

¹Institute of Arctic and Alpine Research, University of Colorado Boulder, Boulder, Colorado, USA, ²Department of Geography, University of Colorado Boulder, Boulder, Colorado, USA, ³Jet Propulsion Laboratory, California Institute of Technology, Pasadena, California, USA

Abstract We used multiple sources of remotely sensed and ground based information to evaluate the spatiotemporal variability of snowpack accumulation, potential evapotranspiration (PET), and Normalized Difference Vegetation Index (NDVI) throughout the Southern Rocky Mountain ecoregion, USA. Relationships between these variables were used to establish baseline values of expected forest productivity given water and energy inputs. Although both the snow water equivalent (SWE) and a snow aridity index (SAI), which used SWE to normalize PET, were significant predictors of the long-term (1989–2012) NDVI, SAI explained 11% more NDVI variability than SWE. Deviations from these relationships were subsequently explored in the context of widespread forest mortality due to bark beetles. Over the entire study area, NDVI was lower per unit SAI in beetle-disturbed compared to undisturbed areas during snow-related drought; however, both SAI and NDVI were spatially heterogeneous within this domain. As a result, we selected three focus areas inside the larger study area within which to isolate the relative impacts of SAI and disturbance on NDVI using multivariate linear regression. These models explained 66%-85% of the NDVI and further suggested that both SAI and disturbance effects were significant, although the disturbance effect was generally greater. These results establish the utility of SAI as a measure of moisture limitation in snow-dominated systems and demonstrate a reduction in forest productivity due to bark beetle disturbance that is particularly evident during drought conditions resultant from low snow accumulation during the winter.

1. Introduction

Climate warming is changing the way that forested ecosystems function [Bonan, 2008]. Globally, latitudinal gradients in water and energy availability have shifted, and water limitation is becoming characteristic of many historically energy limited forest ecosystems [Bentz et al., 2010; Wu et al., 2012; Anderegg et al., 2014; Buermann et al., 2014; Stinziano and Way, 2014]. Drought in forested ecosystems is thus emerging as a research priority [Clark et al., 2016], and in North America, this shift toward increasing water limitation has been accompanied by notable increases in forest disturbance associated with insect infestation [Safranyik et al., 2010; Hart et al., 2014]. At the regional scale, altitudinal gradients similarly govern resource availability and limitation, and species distribution [Carpenter, 2005], rates of forest productivity [Schimel et al., 2002], and vulnerability to disturbance [Westerling et al., 2006; Logan et al., 2010; Pepin et al., 2015] have all been linked to elevation. The ability of ecosystems to adapt to changes in climate is, in part, dictated by the degree to which species can move geographically to coincide with movement in optimal climatic conditions. However, the rate of climate change in many high latitude and high altitude ecosystems currently exceeds the ability of many long-lived tree species to migrate [Davis and Shaw, 2001]. Hence, these tree species are becoming progressively vulnerable to the direct and indirect effects of drought-related moisture stress associated with climate warming [Kolb et al., 2016].

Several works have documented changes in the magnitude of snow accumulation [Mote et al., 2005; Clow, 2010; Harpold et al., 2012] and the timing of snowmelt [Stewart et al., 2005] in the western United States, with significant implications for forested ecosystems. For example, Trujillo et al. [2012] found a strong positive relationship between the magnitude of winter snow accumulation and summer growing season forest productivity in the Sierra Nevada Mountains of California. Studies at the plot scale in the Colorado Rocky Mountains have also demonstrated an important link between the timing of snowmelt and the onset of the growing season, whereby earlier snowmelt resulted in longer growing seasons [Monson et al., 2002; Hu et al., 2010]. Interestingly, however, these longer growing seasons were associated with decreased growing

© 2017. American Geophysical Union. All Rights Reserved.

season productivity due to late season water stress [Monson et al., 2005; Sacks et al., 2007]. Given that water stress in these forested systems can increase plant attractiveness to insects [Mattson and Haack, 1987; Kelsey et al., 2014] while simultaneously reducing carbohydrate-based tree defenses [Kolb et al., 2016], there is the potential for a positive feedback between severe drought and insect disturbance [e.g., Fettig et al., 2013]. In turn, insect-related forest disturbance impacts the timing and magnitude of snowmelt [Biederman et al., 2012; Pugh and Small, 2012], the hydrology and biogeochemistry of affected watersheds [Edburg et al., 2012; Hicke et al., 2013; Bearup et al., 2014], and water quality [Mikkelson et al., 2013a, 2013b; Vose et al., 2016]. Notwithstanding, a major limitation to observational studies focused on the postdisturbance ecosystem response to drought [e.g., Breshears et al., 2005; Anderegg et al., 2015] is the need to study processes over relatively long time scales such that predisturbance and postdisturbance drought conditions can be studied in tandem to evaluate the differential ecosystem response.

Long-term satellite observations, such as data from the Advanced Very High Resolution Radiometer (AVHRR), represent an invaluable tool with which to gain insight into the forest response to climate change, as the instrumental record of these sensors now exceeds 30 years. Many studies have characterized the sensitivity of satellite-observed visible and near-infrared reflectance measurements to vegetation stress [Angert et al., 2005; Peng et al., 2011]. Based on these reflectance sensitivities, several indices of vegetation productivity have also been identified [Huete et al., 2002]. Similarly, coupled satellite-model-based estimates of vegetation productivity have been derived using Moderate Resolution Imaging Spectroradiometer (MODIS) data, whereby models of land-atmosphere carbon exchange are constrained by land-surface temperature observations [Running et al., 2004; Zhao et al., 2005]. When evaluated at the global scale, these data have been used to inform the ecosystem productivity response to interannual climate variability over relatively short time periods (i.e., since 2000).

Satellite data have also been used to study the relationship between climate variability and associated snowpack dynamics [Guan et al., 2010, 2012]. Snow cover extent has traditionally been mapped using a normalized difference snow index (NDSI), in which a band ratio method is employed using reflectance observations in the visible and near-infrared portions of the spectrum [Dozier, 1989; Hall et al., 1990]. Developments in snow cover detection now afford observations of fractional snow-covered area from Landsat Thematic Mapper data [e.g., Rosenthal and Dozier, 1996] and from MODIS [Hall and Riggs, 2007; Painter et al., 2009; Rittger et al., 2013], and reconstructions of snow water equivalent (SWE) have now been conducted at small headwater catchment scales [e.g., Molotch and Bales, 2006; Jepsen et al., 2012] and at the mountain range scale [e.g., Guan et al., 2013; Cornwell et al., 2016] using this technology. While these SWE estimates present a significant opportunity for evaluation of the hydrologic impacts of disturbance, little work has been done to leverage the long history of snow remote sensing in the context of ecosystem disturbance. To address this, we introduce the snow aridity index as a metric that incorporates the combined effects of moisture availability (SWE) and demand (potential evapotranspiration) on vegetation productivity.

Combining the aforementioned remotely sensed data sets, this study investigates relationships between forest productivity as measured via Normalized difference vegetation index (NDVI; dependent variable) and seasonal snow accumulation, potential evapotranspiration (PET), a snow aridity index, and cumulative forest mortality (independent variables). We hypothesize that the snow aridity index may represent a particularly robust predictor of vegetation productivity since it incorporates the air temperature-dependent impacts of increased vapor pressure deficit and reduced snowfall fraction that are among the most well-established effects of climatic change [Luce et al., 2016; Novick et al., 2016]. Moreover, moisture availability is likely to be determined to a greater degree by precipitation relative to evapotranspiration (ET) in snow-dominated ecosystems [Vose et al., 2016]. We specifically consider three research questions: (1) How does the snow aridity index compare to snow water equivalent as an interannual predictor of peak growing season NDVI? (2) How do these relationships change in the presence of widespread bark beetle disturbance? And (3), to what degree is NDVI influenced by climate (e.g., snow aridity) versus disturbance? These questions are addressed across the Southern Rocky Mountain ecoregion (SRME) and within three nested focus areas where the spatiotemporal variability of forest mortality was well constrained.

2. Study Area

2.1. Southern Rocky Mountain Ecoregion

This research was focused on areas within the SRME [Commission for Environmental Cooperation, 1997; United States Environmental Protection Agency, 2010] located higher than 1500 m above sea level (asl)

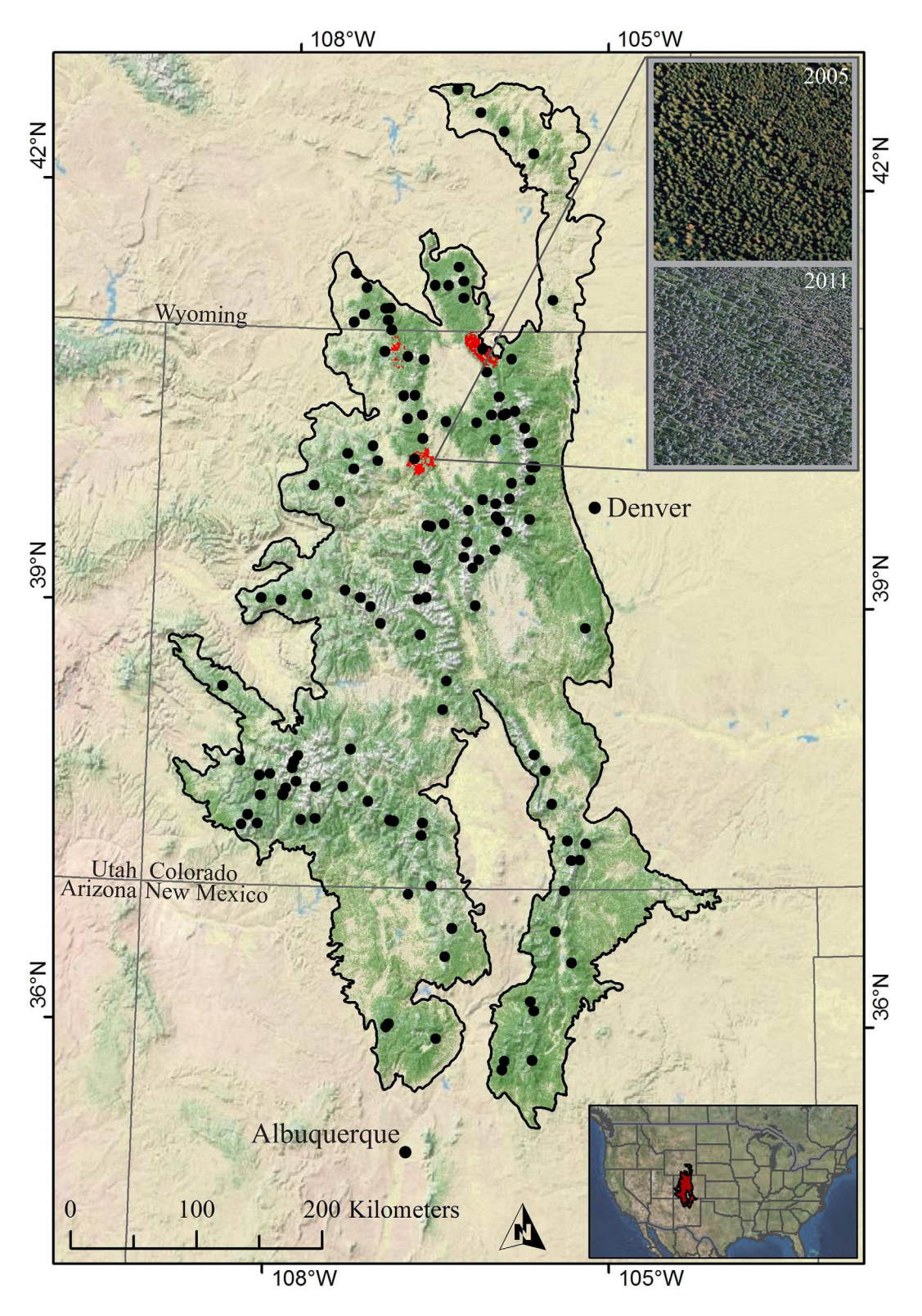


Figure 1. Green areas are USGS NLCD evergreen forests above 1500 m elevation, black dots are NRCS SNOTEL sites, red areas are the three focus areas that were used to constrain the effects of disturbance, and the black outline is the boundary of the Southern Rocky Mountain ecoregion. Focus Area 1 is the most easterly focus area, Focus Area 2 is the most southerly, and Focus Area 3 is the most westerly. The upper inset shows representative vegetation mortality due to bark beetle disturbance within Focus Area 2, where peak mortality occurred in 2007.

(Figure 1). The SRME covers 144,462 km² and spans an area that includes southern Wyoming, Colorado, and northern New Mexico, which represents the headwaters of several major river systems, including the Platte, Colorado, Arkansas, and Rio Grande Rivers. Vegetation in the region consists of a mixture of lower-elevation grasslands, mid-elevation montane forests, higher-elevation mixed conifer and aspen subalpine forests, and a mixture of alpine tundra, exposed bedrock, talus, and isolated glaciers above treeline. To maintain consistency with forest disturbance by bark beetles, analyses were masked to include only areas with evergreen forests as determined by the Landsat-based U.S. Geological Survey (USGS) 2001 National Land Cover Database (NLCD) data (http://www.mrlc.gov/nlcd2001.php) [Homer et al., 2007]. The NLCD data were upscaled from 30 m to 1 km cell size for consistency with the remotely sensed NDVI data from AVHRR. Aggregation to 1 km resolution was performed based on the percentage of 30 m evergreen cells inside each 1 km cell such that the resulting evergreen mask contained only areas with greater than 50% evergreen forest cover. Principal tree species (from approximately north to south) included Engelmann spruce (*Picea engelmanii*), subalpine fir (*Abies lasioscarpa*), lodgepole pine (*Pinus contorta*), limber pine (*Pinus flexilis*), Douglas fir (*Pseudotsuga menziesii*), blue spruce (*Picea pungens*), white fir (*Abies concolor*), ponderosa pine (*Pinus ponderosa*), and southwestern white pine (*Pinus strobiformis*).

2.2. Focus Areas

We also utilized the United States Forest Service (USFS) Aerial Detection Survey (ADS) data to select three smaller focus areas consisting of contiguous or nearly contiguous polygons that experienced exceptional mortality in one single year (Figure 1). In this way, we were able to unambiguously observe the productivity response to snow aridity pre- and post-mortality. Specifically, Focus Area 1 (301 km²), Focus Area 2 (168 km²), and Focus Area 3 (67 km²) were carefully chosen to represent forested areas that contained only endemic bark beetle populations before peak mortality occurred in 2007. The latitude and longitude at the centers of Focus Areas 1, 2, and 3 were 40°52.5'N; 106°4.3'W, 40°3.8'N; 106°37.1'W, and 40°50.6'N; 106°51.7′W, respectively, and the elevation within each focus area ranged from 2300 to 3200 m asl. Focus Area 1 contained 89% lodgepole pine-dominated evergreen forest, 6% herbaceous wetlands, and 1% each of woody wetlands and deciduous forest (mostly quaking aspen, Populus tremuloides). Focus Area 2 contained 85% lodgepole pine-dominated evergreen forest, 6% herbaceous wetlands, 5% deciduous forest, and 2% woody wetlands. Focus Area 3 contained 75% lodgepole pine-dominated evergreen forest, 11% deciduous forest, 6% herbaceous wetlands, 4% mixed forest (neither evergreen nor deciduous trees represent more than 75% of tree cover), and 3% scrubland. Each focus area contained small areas of open water and barren land. Although the USFS ADS data included several bark beetle species, mountain pine beetle (Dendroctonus ponderosae) uniquely occurred in the focus areas.

3. Methods and Data

To address research question 1, we used basic linear regression models to evaluate the long-term (1989–2012) relationship between maximum growing season (1 April to 31 August) NDVI (dependent variable) and both annual maximum SWE and a snow aridity index (SAI) (independent variables) from undisturbed (with respect to fire and insects) areas:

$$NDVI = a + b \times SWE$$
 (1)

$$NDVI = a + b \times SAI$$
 (2)

where *a* and *b* are the intercept and slope of the resulting best fit trendlines, respectively. In this context, SAI is analogous to the aridity index (PET/precipitation) [*Budyko*, 1974], where the SAI was estimated as the sum of 1 April to 31 August potential evaporation (PE) divided by annual maximum SWE from the preceding spring. Equations (1) and (2) were additionally calculated with low SWE or SAI years excluded in order to assess the influence of statistical outliers [*Cook*, 1979].

To address research question 2, we utilized a before-after-control-impact sampling design to determine the effect of bark beetles on NDVI over the same 1989–2012 period:

$$NDVI(BB) = a + b \times NDVI(U) + c \times Disturbance[0, 1] + d \times (NDVI(U) \times Disturbance[0, 1])$$
 (3)

where *U* and *BB* represent undisturbed and beetle-disturbed areas, *b*, *c*, and *d* correspond to the change in NDVI per unit increase in each independent variable, and *Disturbance* is a binary variable corresponding to

greater than (disturbed) or less than (undisturbed) 70% forest mortality per the ADS data. We then used multivariate regression analysis of the presence/absence of disturbance, the SWE or SAI, and their interaction (independent variables) to further quantify the separate and combined impacts of climate and disturbance on NDVI (dependent variable) (research question 3):

$$NDVI = a + b \times SWE + c \times Disturbance [0, 1] + d \times (SWE \times Disturbance [0, 1])$$
 (4)

$$NDVI = a + b \times SAI + c \times Disturbance [0, 1] + d \times (SAI \times Disturbance [0, 1])$$
 (5)

Companion analyses used a continuous measure of percent cumulative tree mortality (*Mortality*) [*Meddens et al.*, 2012] to additionally evaluate research questions 2 and 3 between 2000 and 2012 using MODIS satellite data [*Didan*, 2015] at the focus area scale:

$$NDVI = a + b \times SWE + c \times Mortality + d \times (SWE \times Mortality)$$
 (6)

$$NDVI = a + b \times SAI + c \times Mortality + d \times (SAI \times Mortality)$$
 (7)

where SAI was calculated as PET/SWE. Different sources of SWE and PET or PE information were used for the shorter-term and longer-term analyses to take advantage of the best available data, including multiyear composites of SWE and SAI that were created from the longer-term data, in recognition of the potential for interannual lags in the effect of moisture availability on vegetation productivity [Kirchner, 2016]. Specifically, both SWE and SAI were calculated as variable blends (in increments of 5%) of SWE and SAI from the current year (50%–70%), the previous year (20%–40%), and 2 years prior (10%–20%) for the 1989–2012 regressions. The resulting data are presented as mean values of all possible lag combinations with the corresponding range of R² and p values among all possible blends. The shorter-term focus area analyses were not subject to this lagging procedure in order to preserve the maximum length of the MODIS data record. In this sense, the analyses during the AVHRR time period afford a longer-term view of the forest response to snow aridity, whereas the MODIS data allow for more detailed spatial analyses since PET, SWE, and tree mortality data are available for each pixel in the domain over the MODIS time period. Further details regarding these analyses and data sets are provided below.

3.1. AVHRR-Based Analyses

3.1.1. AVHRR NDVI Data

The AVHRR NDVI data set used for our longer-term (1989–2012) analyses was based on the USGS AVHRR NDVI (https://lta.cr.usgs.gov/NDVI) record. These data were derived from AVHRR-observed reflectance data in the red and the near-infrared portions of the electromagnetic spectrum and were produced on 2 week intervals at 1 km spatial resolution. The maximum annual growing season (1 April to 31 August) NDVI was uniquely determined for each AVHRR pixel. In this way, we account for pixel-to-pixel temporal variations in the occurrence of maximum NDVI within a given year, as the timing of maximum NDVI can vary from one pixel to another. To prevent contamination of the NDVI values due to the presence of snow cover, AVHRR acquisitions during the snow-covered season were not included in the calculation of maximum growing season NDVI.

3.1.2. NLDAS-2 Potential Evaporation Data

The 1 April to 31 August monthly PE was obtained from NASA's North American Land Data Assimilation System Phase 2 (NLDAS-2; http://disc.sci.gsfc.nasa.gov/hydrology/data-holdings) [Mitchell et al., 2004; Xia et al., 2012], downscaled from 11 to 1 km spatial resolution by resampling each pixel to an 11 km \times 11 km grid of 1 km grid cells (original 11 km value applied to all 1 km cells), and cumulatively summed. This PE is derived from the National Centers for Environmental Prediction (NCEP) North American Regional Reanalysis (NARR) analysis fields where the PE is calculated using the modified Penman scheme of Mahrt and Ek [1984].

3.1.3. Snow Telemetry Snow Water Equivalent Data

SWE data were acquired on a daily basis from the United States Natural Resource Conservation Service (NRCS) SNOTEL network (ftp.wcc.nrcs.usda.gov/data/snow/snotel/cards) [*Trujillo and Molotch*, 2014], and maximum SWE values were identified for each water year between 1989 and 2012 (the length of the NDVI data set). A total of 131 SNOTEL stations were included in this analysis; however, stations were excluded for any year in which a valid maximum SWE could not be determined.

3.2. MODIS-Based Analyses

3.2.1. MODIS NDVI Data

MODIS-based 1 km NDVI estimates (MOD13A3) were obtained from the NASA Land Distributed Active Archive [Didan, 2015]. These data are produced as 16 day temporal resolution composites of daily data, which provides spatially continuous greenness estimates devoid of data gaps due to cloud cover or poor viewing geometry. From the 16 day data, monthly NDVI values are generated using a time-weighted average of the reflectance fields in the 16 day products. This 16 day product includes atmospherically corrected MODIS bidirectional reflectance measurements from both the Terra and Aqua satellites, which have been composited based on a variety of quality assurance metrics to exclude low quality pixels. In addition, the standard product-generation methodology includes a viewing geometry filter whereby the two highest NDVI values were determined and then the value acquired closest to nadir is selected [Didan, 2015]. Calculation of the maximum annual growing season MODIS NDVI was equivalent to the AVHRR procedure described in section 3.1.1.

3.2.2. MODIS Potential Evapotranspiration Data

Monthly MODIS-based estimates of PET at 1 km resolution were generated by temporal averaging of the MODIS 8 day ET data products (MOD16A2) [*Mu et al.*, 2011]. PET estimates were based on the Penman-Monteith equation forced by both ancillary meteorological data and 8 day MODIS-based vegetation information. The MODIS PET product is generated using four MODIS-based data sources including 8 day composites of Fractional Absorbed Photosynthetically Active Radiation (FPAR), 8 day land surface albedo, 8 day Leaf Area Index (LAI), and land cover type. The 8 day albedo composites were combined with daily surface solar irradiance and air temperature data from meteorological reanalysis to derive the surface net radiation and ground heat flux [*Mu et al.*, 2011]. Surface stomatal conductance and aerodynamic resistance were estimated from a combination of MODIS LAI and reanalysis of daily air temperature, vapor pressure deficit (VPD), and relative humidity. Biome-dependent vegetation parameters were obtained from MODIS-based land cover information. These parameters were optimized such that annual ET estimates for each biome agreed with ET estimates based on MODIS-derived Gross Primary Productivity (GPP) and known water use efficiencies established from eddy covariance measurements [*Mu et al.*, 2011].

3.2.3. MODIS SWE Reconstruction Data

The SWE reconstruction model [Molotch et al., 2004; Molotch, 2009; Guan et al., 2013; Schneider and Molotch, 2016] uses calorimetry to reconstruct SWE on a daily basis from maximum snow accumulation in late winter throughout the snowmelt season. For this model, calculations were made on a pixel-by-pixel basis, in which modeled snowpack-atmosphere energy exchange was integrated over the period of MODIS-observed snow-covered area. Surface-atmosphere energy fluxes were calculated based on a one-layer snow model that assumes an infinite snow depth to derive estimates of potential snowmelt flux. The potential snowmelt flux was then scaled by pixel-specific estimates of fractional snow-covered area (SCA) derived from the MODIS instrument. The MODIS SCA estimates were in turn derived from the MODIS Snow Covered Area and Grain Size Algorithm (MODSCAG) [Painter et al., 2009], which uses a least squares approximation to estimate SCA for each pixel using MODIS bands 4 and 6. Spectral unmixing is conducted based on 30 modeled snow spectra and baseline soil, rock, and vegetation spectra [Painter et al., 2009]. Snow-atmosphere energy exchange was modeled using an explicit characterization of radiative fluxes in which NLDAS estimates of solar irradiance were downscaled by a geometric terrain reflectance model [Dozier and Frew, 1990], surface albedo was parameterized based on snow age [Dickinson et al., 1993], and net longwave radiation was calculated based on topographically downscaled NLDAS estimates of vapor pressure and air temperature. In this regard, values of longwave radiation were estimated using the Stefan-Boltzmann equation in which the emissivity of the atmosphere was determined from estimates of air temperature and water vapor pressure [Idso, 1981; Hodges et al., 1983]. Turbulent fluxes were explicitly calculated using the bulk transfer method of Jordan [1991], with a bulk Richardson number from Liston [1999]. Stability corrections were applied during both stable and unstable turbulent conditions and forcings were derived from terrain-downscaled NLDAS estimates of wind speed, air temperature, and vapor pressure. Further details on the SWE reconstruction model, MODSCAG data, model forcings, and downscaling procedures can be found in Guan et al. [2013].

3.2.4. Disturbance Masks

For both the AVHRR and MODIS analyses, areas of disturbance were identified, and disturbance masks were created, using the USFS ADS data. The USFS Aerial Detection Surveys estimated forest mortality based on

Table 1. Specific Attributes of Data Collection, Processing, Application, and Products (Figures)						
Geographical		Time	Disturbance	Research		
Area	Instrument	Period	Mask	Question(s)	Equations	Figure(s)
Ecoregion	AVHRR	1989–2012	Dynamic	1	1–2	2
Ecoregion	AVHRR	1989-2012	Static	2–3	3–5	3
Ecoregion	MODIS	2000-2012	n/a	3	n/a	4–5
Focus areas	MODIS	2000–2012	Dynamic	2–3	6–7	6

manual observations from aircraft wherein visual estimates of dead trees were obtained and transcribed manually onto a base map. When converting the polygons from vector to raster format, only raster cells containing more than 70% coverage of mortality polygons were included in the disturbance mask. In this way, the ADS data were used only as an index of the presence/absence of disturbance. When relative differences in vegetation mortality were considered (e.g., the focus area analysis), a standardized (for host species type and crown area) ADS product was used [Meddens et al., 2012]. Since the SRME straddles two USFS regions, digital tree mortality data starts in 1993 in Colorado and Wyoming, but not until 1996 for New Mexico. The year of forest mortality was estimated by subtracting one year from the survey date. This 1 year subtraction was necessary given that trees are in the red phase when they are detected and therefore represent the year after initial mortality. To address research question 1, spatially variable disturbance masks were created wherein a unique set of disturbed polygons was selected for each year, each annual polygon layer was cumulatively summed, and then each cumulative annual polygon layer was converted to a 1 km gridded raster layer to coincide with the cell size of the MODIS and AVHRR satellite imagery. For research questions 2 and 3, ecoregion-scale disturbance masks remained spatially fixed at the maximum and minimum extents of disturbed and undisturbed areas, respectively, which occurred in 2012. In this way, disturbed areas experienced progressively more mortality through time, which when compared to undisturbed areas on an interannual basis, allows for calculation of the disturbance impact and separation of the relative climatic versus disturbance influences on NDVI. The disturbance masks created to investigate research questions 2 and 3 at the focus area scale were analogous to those used for research question 1, but restricted to areas within the geographical boundary of each focus area (Table 1).

4. Results

4.1. AVHRR-Based Analyses

The USGS AVHRR NDVI time series was significantly correlated with the SNOTEL-observed annual maximum SWE (mean $R^2=0.29$; mean p=0.01) (Figure 2a) and the R^2 values resultant from regressions of the temporally-lagged combinations of SWE on NDVI ranged from 0.24 to 0.33 (0.004 $). However, when the two snow drought years (2002 and 2012) were removed from this analysis, the undisturbed SWE was a weaker predictor of NDVI (mean <math>R^2=0.17$; mean p=0.06). The maximum annual SWE from undisturbed areas averaged 467 mm (standard deviation (σ) = 99 mm) and the highest SWE was observed in 1993 (659 mm), which coincided with the maximum NDVI value during the AVHRR time period (0.70). The lowest SWE occurred in 2002 (255 mm) and corresponded to the second-lowest AVHRR-observed NDVI value of 0.60.

The SAI was a better predictor of NDVI than the SWE (mean $R^2=0.40$; mean p<0.001) (Figure 2b), and the relationship between SWE (independent variable) and SAI (dependent variable) was well described by a concave up second degree polynomial ($R^2=0.96$; $p\ll0.001$). The R^2 values resultant from regressions of the temporally-lagged combinations of SAI on NDVI ranged from 0.35 to 0.44 (<0.001 < p<0.002). Importantly, the SAI was still a significant predictor of NDVI (mean $R^2=0.20$; mean p=0.04) when the snow drought years were removed from this analysis. The undisturbed SAI averaged 2.1 ($\sigma=0.6$) and the maximum SAI of 3.8 occurred in the minimum NDVI year of 2012. In contrast, the minimum SAI (1.2) occurred in 1997, which had an NDVI value very close to the mean at 0.66. The persistent negative relationship between SAI and NDVI demonstrates that the link between vegetation productivity and water availability is maintained during periods of both typical and extreme climate variability (Figure 2b).

Figure 3a compares the long-term NDVI from an undisturbed area (40,255 km²) to an area that was progressively impacted by bark beetles (13,796 km²) to explore the cause of the unexplained variance in Figure 2.

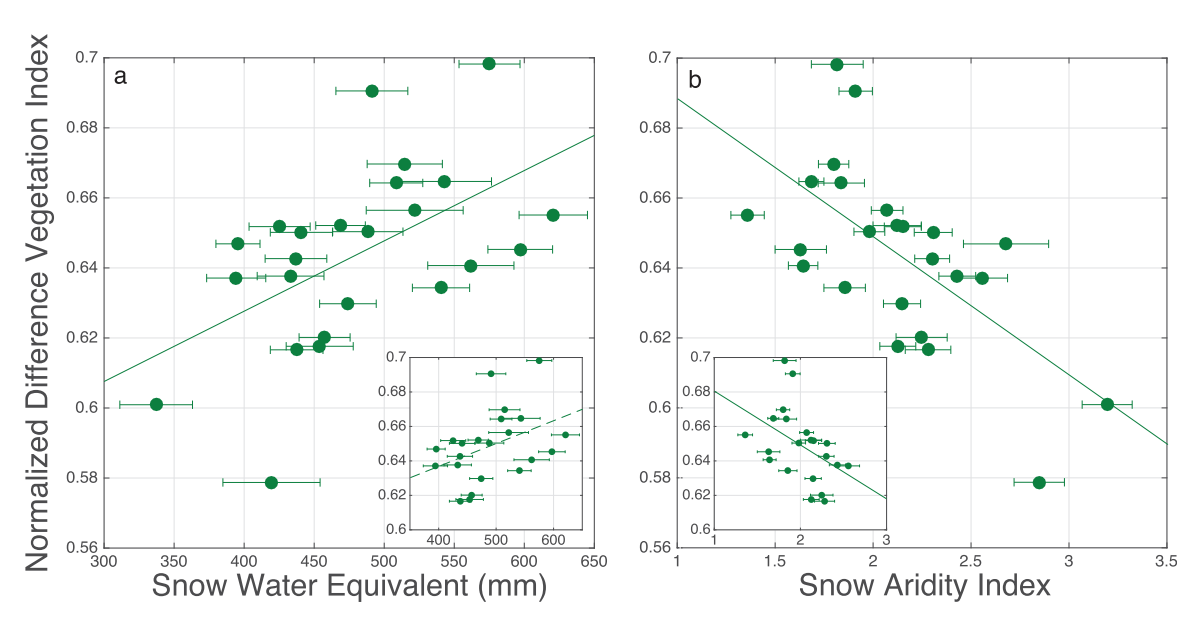


Figure 2. Ecoregion-scale AVHRR-NDVI as a function of (a) SWE and (b) SAI. Insets show the same relationships with low SWE or SAI (snow drought) outliers removed. Solid lines denote significant (p < 0.05) regressions.

Even before widespread disturbance began in 2006, the maximum growing season AVHRR-NDVI was 6% higher in the progressively disturbed (0.67; σ = 0.06) compared to the undisturbed (0.63; σ = 0.08) area, which likely corresponds to the presence of higher-density forest stands that are especially prone to bark beetle invasion [*Raffa et al.*, 2005]. While the undisturbed NDVI was a significant predictor of the progressively disturbed NDVI both before (p < 0.001) and after (p = 0.002) disturbance began in 2006, multivariate regression of the undisturbed NDVI (p < 0.001), a binary disturbance indicator (*Disturbance*; p = 0.06), and their interaction (p = 0.07) (equation (3)) on the progressively disturbed area NDVI showed that the slope of this relationship was greater postdisturbance (Figure 3a). Furthermore, the predisturbance and

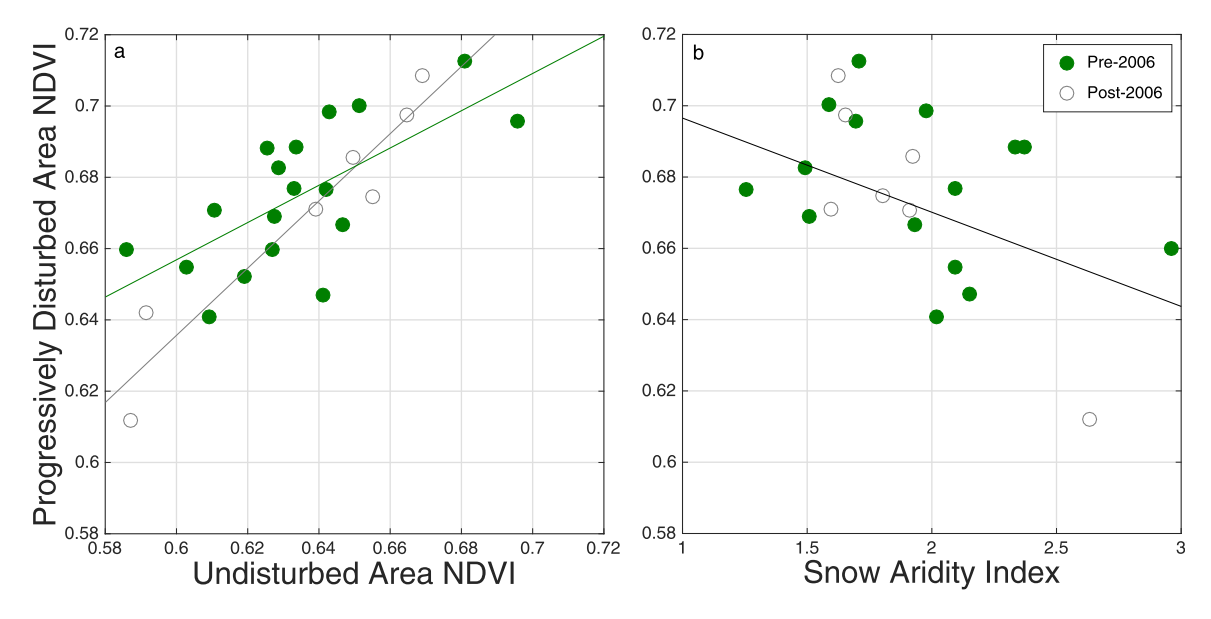


Figure 3. (a) Comparison of ecoregion-scale AVHRR NDVI between control (40,255 km²) and progressively disturbed (13,796 km²) areas before (green line) and after (gray line) widespread bark beetle disturbance began in 2006 shows reduced NDVI in disturbed areas when NDVI is less than 0.65. The following equation (equation (3)) explained 68% of the variance (p < 0.001) in the progressively disturbed area NDVI: $y = 0.070 + 0.94 \times \text{Undisturbed NDVI} + 0.27 \times \text{Disturbance}[0,1] - 0.42 \times (\text{Undisturbed NDVI} \times \text{Disturbance}[0,1])$ where Disturbance is a binary indicator of widespread bark beetle disturbance that was set to zero prior to 2006 and one thereafter. (b) Multivariate regression (equation (5)) of the snow aridity index and Disturbance is shown by the black line and explained 44% of the variance (p = 0.01) in the progressively disturbed area NDVI: $y = 0.82 - 0.077 \times \text{SAI} - 0.11 \times \text{Disturbance}[0,1] + 0.062 \times (\text{SAI} \times \text{Disturbance}[0,1])$.

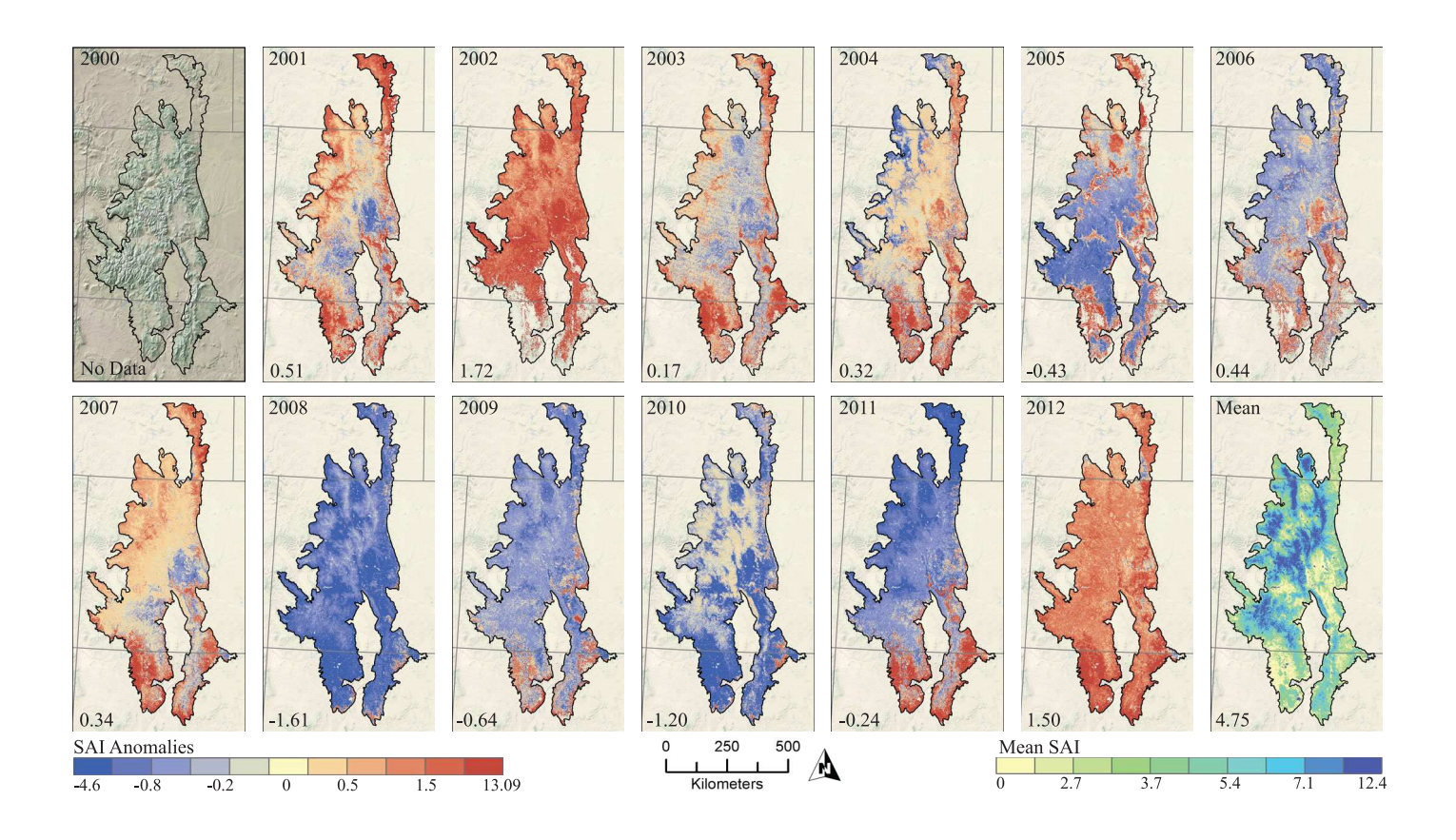


Figure 4. Spatial analysis of the annual MODIS-derived snow aridity index (SAI) anomalies (lower left corner of each panel) from the long-term mean (shown in the bottom right panel) between 2001 and 2012 throughout the Southern Rocky Mountain ecoregion. The snow aridity index was derived by dividing the summed 1 April to 31 August Potential Evapotranspiration by the 1 March reconstructed SWE.

postdisturbance best fit linear trendlines intersected at an NDVI value of approximately 0.65, which was close to the mean NDVI value (0.64) from undisturbed areas. This result affirms that a measure of disturbance is needed to accurately scale predictions of NDVI based on climatic indices such as the SAI, and further suggests the presence of an NDVI threshold value above (positive effect) and below (negative effect) which disturbance has the opposite effect on NDVI. The NDVI was therefore modeled using SWE (equation (4)) or SAI (equation (5)) and the binary disturbance indicator within this same progressively disturbed area. For the SWE/disturbance multivariate regression model, none of the individual terms were significant (p > 0.19) and overall, this model was not a significant predictor of NDVI (p = 0.47). In contrast, the SAI (p = 0.003), disturbance (p = 0.03), and interaction (p = 0.02) terms in the SAI/disturbance model explained 44% (p = 0.01) of the NDVI variability and corroborated that the relationship between SAI and NDVI changes in the presence or absence of disturbance (Figure 3b).

4.2. MODIS-Based Analyses

The MODIS data were used to investigate the degree to which the spatial variability of snow aridity and vegetation greenness throughout the SRME could represent an additional source of uncertainty. The MODIS-estimated SAI values depicted patterns of snow-related drought intensity as evidenced by the spatially distributed anomaly from the mean annual SAI (Figure 4). The majority of years showed a mixture of negative and positive SAI anomalies throughout the SRME, illustrating the heterogeneity associated with synoptic-scale meteorology and complex topography in this study area. There was a significant ($R^2 = 0.36$; p = 0.04) relationship between the SAI and MODIS NDVI but not between the SWE and MODIS NDVI (p = 0.21) that likely resulted from the relatively short 13 year MODIS record used in this study. Corollaries between SAI and NDVI were observed in 2008 and 2010 when the SAI anomaly was overwhelmingly negative (Figure 4) and the NDVI anomaly was positive (Figure 5); note the southern portion of the domain where the SAI and NDVI anomalies were greater in magnitude. Similarly, during the drought years of 2002 and 2012, positive

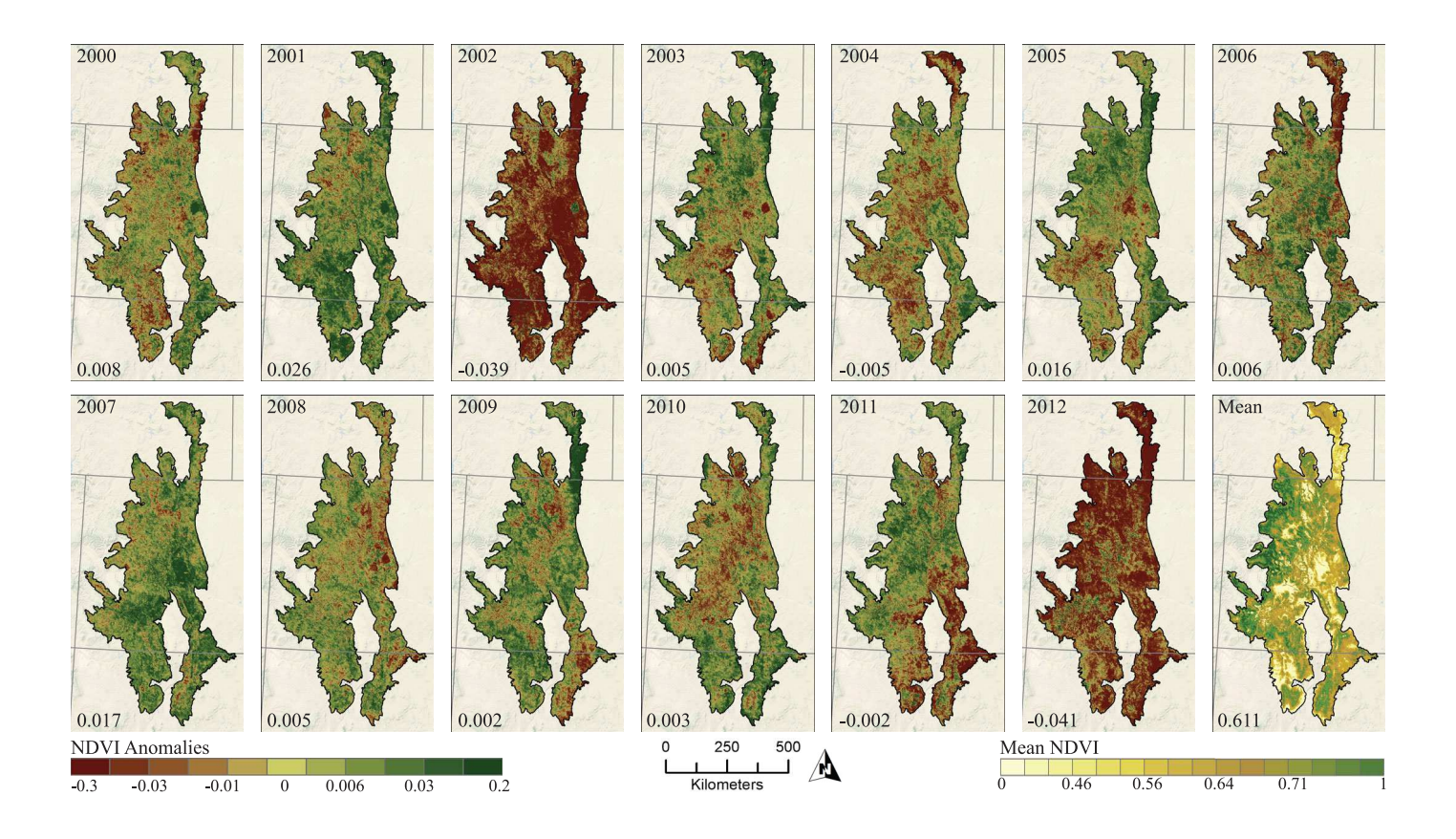


Figure 5. Spatial analysis of (bottom right) the mean MODIS-observed peak growing season NDVI and (lower left corner of each figure) the annual anomaly from that mean between 2000 and 2012 throughout the Southern Rocky Mountain ecoregion.

SAI anomalies and snow-related drought conditions prevailed throughout nearly the entire SRME (Figure 4), and commensurate negative NDVI anomalies were observed (Figure 5).

Interestingly, spatial differences between the drought years of 2002 and 2012 were apparent wherein the southern SRME SAI was greater in 2012 and the northern SRME SAI was greater in 2002 (Figure 4). The MODIS-observed peak growing season NDVI also exhibited significant interannual variability with wetter years showing positive anomalies and drier years corresponding to negative anomalies (Figure 5). The mean annual MODIS NDVI was 0.61 and the mean annual NDVI anomaly was positive during 9 out of 13 years, which demonstrates that years with low productivity were infrequent but intense during the study period. This interpretation was corroborated by the magnitude of the minimum (–0.041 in 2012) versus the maximum (0.026 in 2001) mean annual NDVI anomaly. Comparing between the 2002 and 2012 drought years, the NDVI anomaly was shifted geographically, with the southern part of the domain showing a more negative anomaly in 2002, in contrast to 2012, when the NDVI anomaly was most negative in the northern part of the SRME. Beginning in 2008, a persistent negative NDVI anomaly can be seen in the northern part of the domain, which is consistent with the progression of insect-related mortality in that part of the region; i.e., bark beetles caused considerably more forest mortality in the northern versus southern part of the domain.

Given the spatial heterogeneity of SAI and NDVI throughout the SRME, we narrowed our analysis to the focus area scale. In this context, we were able to control for the effects of vegetation, climatic variability, and disturbance history by considering only a well-defined area that experienced widespread disturbance over a relatively short period of time. Cumulatively, the focus areas had between 83% and 91% dead trees per pixel [Meddens et al., 2012], and annual vegetation mortality peaked in 2007 in all three focus areas (Figure 6a). There was a significant (p < 0.03) inverse relationship between tree mortality and the NDVI within each focus area (Figure 6b), and before peak mortality occurred, there was also a significant (p < 0.03)

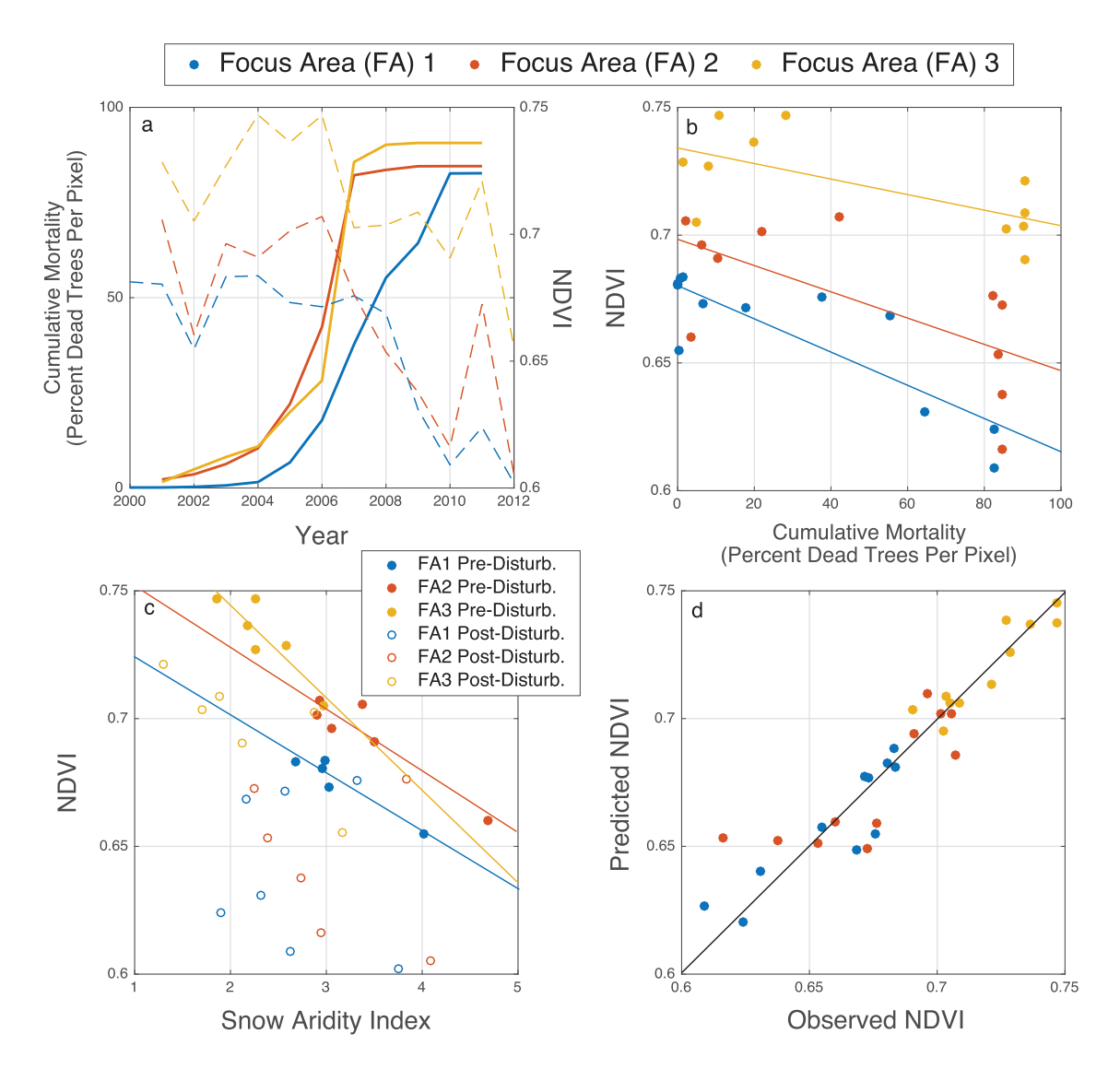


Figure 6. (a) Time series analysis of cumulative mortality (solid lines) and NDVI (dashed lines) for Focus Areas 1–3. Focus area NDVI (vertical axis) plotted against (b) cumulative mortality and (c) the snow aridity index before and after bark beetle disturbance peaked in 2007. (d) Observed NDVI (horizontal axis) plotted versus NDVI predicted from a multiple linear regression with cumulative mortality and SAI as dependent variables; black line represents the 1:1 relationship. Cumulative mortality data (Figures 6a and 6b) are taken from *Meddens et al.* [2012] and colored regression lines denote significant relationships.

inverse relationship between the MODIS-derived SAI and NDVI that was representative of a dominant influence of snow aridity on NDVI (Figure 6c). Postdisturbance, however, this relationship deteriorated in Focus Areas 1 and 2 where the SAI and NDVI were no longer significantly correlated; the SAI remained a predictor (p=0.06) of the (albeit lower) postdisturbance NDVI in Focus Area 3. Comparison of the predisturbance versus postdisturbance SAI-NDVI relationship at the focus area scale further constrains the degree to which the NDVI declined per unit SAI postdisturbance (Figure 6c). Beginning in 2008, the (SAI-normalized) postdisturbance NDVI was persistently lower than the pre-disturbance SAI/NDVI relationship would predict, and the cumulative mortality was a significant (0.01) predictor of the NDVI reduction per unit SAI in each of the three focus areas (data not shown). Results of the multivariate regression analysis indicated that SAI and cumulative tree mortality (<math>p < 0.1 for both terms in all focus areas) explained the NDVI variability better than SWE and cumulative tree mortality within each focus area, and Figure 6d compares the results of this analysis to the 1:1 line. Overall, multivariate regression analysis of SAI and the cumulative tree mortality explained between 66% and 85% of the NDVI variability. Between the three focus areas, beta coefficients from the multiple linear regression analysis show that the cumulative mortality term explained 1.3 to 3.7 times more of the observed NDVI variability than the SAI term.

5. Discussion

In the absence of disturbance, the SAI metric was a better predictor of NDVI compared to the SWE, and the SAI explained 40% of the NDVI variance in undisturbed regions within the SRME between 1989 and 2012. Although previous work has had success using SWE to predict remotely sensed NDVI [*Trujillo et al.*, 2012], vegetation water stress has been shown to result from a spatiotemporally variable combination of (soil moisture) supply and (atmospheric) demand in snow-dominated systems where productivity may be seasonally or even sporadically limited by moisture [*Emanuel et al.*, 2010; *Luce et al.*, 2016; *Novick et al.*, 2016]. In contrast to SWE, the SAI explicitly incorporates a measure of each of these conditions, and as a result, the SAI predicted 11% more of the NDVI variability in undisturbed areas throughout the SRME. Based on this positive result, we put forth the SAI as a relatively simple metric with which to quantify moisture limitation, providing an ability to compare the productivity response to droughts of varying intensity from a variety of snow-dominated systems. As an analog to the well-established aridity index, we especially encourage future work to investigate the utility of the SAI to Budyko-style analyses from snow-dominated catchments [e.g., *Berghuijs et al.*, 2014; *Knowles et al.*, 2015; *Barnhart et al.*, 2016].

These results join a growing body of literature to suggest that the productivity response to moisture stress can be fundamentally altered by disturbance [e.g., McDowell et al., 2008; Bentz et al., 2010]. At the ecoregion scale, we observed lower NDVI in disturbed relative to undisturbed areas below approximately the mean NDVI (Figure 3a), as well as lower NDVI per unit SAI in the presence of widespread disturbance (Figure 3b). A similar phenomenon was observed at the focus area scale whereby NDVI was lower than predicted by the combination of SAI and cumulative mortality during four out of the five lowest NDVI years (Figure 6d). We identify two physical mechanisms as potential causes of this phenomenon: (1) the occurrence of an initial drought (in 2002) that "primed" the forest such that it was particularly susceptible to additional disturbance [Gaylord et al., 2013; Hart et al., 2014] and/or (2) interaction between moisture-induced and disturbanceinduced stress that combined in a nonadditive way [Anderegg et al., 2015]. Within this framework, we attribute our inability to identify a significant nonlinear postdisturbance SAI-NDVI relationship to the short postdisturbance NDVI record and in particular, the lack of high-NDVI years during this time. Notwithstanding, forests in the SRME are likely to be more affected by drought in the future (due to both increased PET and decreased SWE), hence these tipping points in forest productivity may play a progressively greater role in dictating ecosystem services in the future. Here we quantify the reduction in forest productivity that can be expected from the separate and combined influences of snow drought and insect disturbance, which represents an important feedback to climate change. Additionally, the indirect effects of drought-induced or disturbance-induced reductions in forest productivity have been shown to extend to species composition [Pec et al., 2015], nutrient cycling [Edburg et al., 2011], and water resources [Reed et al., 2014; Sun et al., 2015]. Most importantly, this analysis suggests that drought and disturbance thresholds may exist, whereby the productivity response to moisture provided by snowmelt is severely curtailed.

Spatial analysis of the annual SAI and NDVI anomalies (differences from the long-term mean) over time offers additional insight into our regression modeling results. For example, Figure 4 shows the annual SAI anomaly and the snow-related drought years of 2002 and 2012 are clearly visible, as well as the minimum SAI years of 2008 and 2010. In contrast, however, the majority of years show divergent patterns of SAI across the SRME, with areas both above and below the mean in the same year (e.g., 2003, 2005, 2006, 2011). Although this may facilitate identification of regional snow-related drought patterns by looking at similarities between years (e.g., similar SAI anomaly distributions in 2001, 2003, and 2007 or in 2009 and 2011), this also highlights the difficulty of working at the ecoregion scale, especially in complex terrain where meteorological variability occurs over relatively short horizontal and vertical distances. It is not surprising that the resulting annual NDVI anomaly was also highly variable over space (Figure 5), although the NDVI generally exhibited less regional variability and more fine scale variability than the SAI. For example, while the SAI was nearly uniformly below average throughout the SRME in 2008, there were numerous small areas of above- and below-average NDVI during that same year, including some noticeably larger areas toward the northern and eastern boundaries of the SRME that correspond to the areas most affected by bark beetles. This reinforces the notion that there is no singular control on NDVI, and that modeling studies at the ecoregion scale or larger must account for multivariate systems that respond to ongoing meteorological variability that can be additionally punctuated and subsequently influenced by disturbance.

We acknowledge that several sources of uncertainty affect the data used in this study. In particular, there are inherent uncertainties in the SNOTEL network regarding the broad-scale representation of snowcovered terrain [Molotch and Bales, 2006], as well as representativeness issues at the local scale [Molotch and Bales, 2005; Rice and Bales, 2010; Meromy et al., 2013]. For example, the SNOTEL network under-samples steeper terrain as well as the highest and lowest elevations in the SRME. Notwithstanding, our spatially explicit analysis using MODIS data (e.g., Figures 4 and 5) reduces our reliance on SNOTEL data alone. Estimates of reconstructed SWE used in the MODIS-based analyses also have inherent uncertainties which are well established in the literature [Molotch et al., 2010; Jepsen et al., 2012; Slater et al., 2013]. However, these sources of uncertainty likely have modest impacts on our results because model biases do not exhibit notable differences in spatial structure [Molotch, 2009; Molotch and Margulis, 2008; Guan et al., 2013]. The use of NDVI information as a proxy for ecosystem GPP has limitations in that several factors can cause differences between GPP measurements and satellite-based NDVI measurements, especially in cases where absorbed photosynthetically active radiation is nonlinearly related to NDVI [Gitelson et al., 2006]. Furthermore, postdisturbance NDVI values may have greater sensitivities to soil moisture given a greater area of exposed soils [Huete et al., 1992], and both AVHRR-based and MODIS-based NDVI data have inherent uncertainties associated with cloud cover and the associated compositing methods.

We justify our focus on snowpack information, as opposed to annual precipitation, by recent work demonstrating that snowpack dynamics influenced forest carbon uptake during both the snow ablation and snow-free periods of the growing season at a site within the SRME [Winchell et al., 2016; Hu et al., 2010], but a portion of the unexplained variance in the relationships presented herein is likely due to interannual variability in warm season precipitation and air temperature, as well as nutrient availability. Likewise, given that strong SAI-NDVI relationships suggest water limitation, it is intuitive that productivity from a semiarid ecoregion such as the SRME would express vulnerability to insect disturbance that is also influenced by water-related stress associated with snowmelt inputs [Christiansen et al., 1987; Mattson and Haack, 1987; Assal et al., 2016; Kolb et al., 2016]. On a larger scale, these postdisturbance changes in productivity may also affect the partitioning of snowmelt between runoff and ET, as previous work has estimated that ET declines after tree mortality with commensurate increases in runoff [Livneh et al., 2015]. Similarly, Maness et al. [2012] showed that postdisturbance latent heat fluxes in British Columbia decreased by 19% and sensible heat fluxes increased by 8% following insect disturbance. As a result, this study has broad implications for evaluating possible changes in energy versus water limitation to productivity after disturbance in the SRME.

6. Conclusions

This work leveraged a combination of temporally (AVHRR) and spatially (MODIS) rigorous satellite-derived data sets in order to establish the spatiotemporal link(s) between a snow aridity index and NDVI throughout the Southern Rocky Mountain ecoregion, USA. This baseline water-productivity relationship provided a reference to compare against postdisturbance conditions associated with bark beetles, which showed that this type of disturbance has the potential to supersede moisture stress given sufficient forest mortality. At the ecoregion level, the SAI was a significant predictor of NDVI, and the SAI explained 11% more of the baseline NDVI variability than the SWE alone. In some cases (e.g., Figure 6c), the SAI was still a significant predictor of postdisturbance NDVI; nevertheless, this work demonstrates that a disturbance metric is required to accurately predict NDVI in forests with non-endemic bark beetle populations. Moreover, the NDVI was significantly reduced per unit SAI during postdisturbance drought years. However, multiple linear regression analysis of SAI and cumulative mortality predicted only 44% of the temporal NDVI variability at the ecoregion scale, compared to 66%-85% of the NDVI variability within three well-constrained focus areas. These results indicate that postdisturbance productivity per unit snow aridity can be suppressed during drought conditions but that this behavior is modified over large spatial scales by hydroclimatic variability associated with synoptic-scale meteorology and exacerbated by complex mountain terrain. Since high-elevation forests represent the most productive ecosystems in the western U.S., the differential forest responses to moisture limitation in disturbed versus undisturbed forests, as documented here, may have significant implications for regional-scale terrestrial water and carbon cycling in this area.

Acknowledgments

This research was supported by the USDA/NSF Water Sustainability and Climate Program (grant 2012-67003-19802), the Boulder Creek Critical Zone Observatory (NSF DEB-9810218), the NSF Hydrological Sciences Program (EAR-1141764), and the Niwot Ridge Long Term Ecological Research Program (NSF DEB-1027341). Some of the data used in this study were acquired as part of the mission of NASA's Earth Science Division and archived and distributed by the Goddard Earth Sciences (GES) Data and Information Services Center (DISC). Ernesto Trujillo, Dominik Schneider, and Thomas Painter contributed technical support, and comments by Charles Luce, Theodore Barnhart, and three anonymous reviewers improved the quality of this work. All data are available at ftp:// snowserver.colorado.edu/pub/AGU/ SAI_2017/.

References

- Anderegg, W. R. L., L. D. L. Anderegg, J. A. Berry, and C. B. Field (2014), Loss of whole-tree hydraulic conductance during severe drought and multi-year forest die-off, *Oecologia*, 175(1), 11–23, doi:10.1007/s00442-013-2875-5.
- Anderegg, W. R. L., et al. (2015), Tree mortality from drought, insects, and their interactions in a changing climate, *New Phytol.*, 208(3), 674–683, doi:10.1111/nph.13477.
- Angert, A., S. Biraud, C. Bonfils, W. Buermann, J. Pinzon, C. J. Tucker, and I. Fung (2005), Drier summers cancel out the CO₂ uptake enhancement induced by warmer springs, *Proc. Natl. Acad. Sci. U. S. A., 102*(31), 10,823–10,827.
- Assal, T. J., P. J. Anderson, and J. Sibold (2016), Spatial and temporal trends of drought effects in a heterogeneous semi-arid forest ecosystem, For. Ecol. Manage., 365, 137–151, doi:10.1016/j.foreco.2016.01.017.
- Barnhart, T. B., N. P. Molotch, B. Livneh, A. A. Harpold, J. F. Knowles, and D. Schneider (2016), Snowmelt rate dictates streamflow, *Geophys. Res. Lett.* 43, 8006–8016, doi:10.1002/2016GI.069690
- Bearup, L. A., R. M. Maxwell, D. W. Clow, and J. E. McCray (2014), Hydrological effects of forest transpiration loss in bark beetle-impacted watersheds, *Nat. Clim. Change*, 4(6), 481–486, doi:10.1038/nclimate2198.
- Bentz, B. J., J. Régnière, C. J. Fettig, E. M. Hansen, J. L. Hayes, J. A. Hicke, R. G. Kelsey, J. F. Negron, and S. J. Seybold (2010), Climate change and bark beetles of the western United States and Canada: Direct and indirect effects, *BioScience*, 60(8), 602–613, doi:10.1525/bio.2010.60.8.6.
- Berghuijs, W. R., R. A. Woods, and M. Hrachowitz (2014), A precipitation shift from snow towards rain leads to a decrease in streamflow, *Nat. Clim. Change*, 4, 583–586, doi:10.1038/nclimate2246.
- Biederman, J. A., P. D. Brooks, A. A. Harpold, D. J. Gochis, E. Gutmann, D. E. Reed, E. Pendall, and B. E. Ewers (2012), Multiscale observations of snow accumulation and peak snowpack following widespread, insect-induced lodgepole pine mortality, *Ecohydrology*, 7(1), 150–162, doi:10.1002/eco.1342.
- Bonan, G. B. (2008), Forests and climate change: Forcings, feedbacks, and the climate benefits of forests, *Science*, *320*, 1444–1449, doi: 10.1126/science.1155121.
- Breshears, D. D., et al. (2005), Regional vegetation die-off in response to global-change-type drought, *Proc. Natl. Acad. Sci. U. S. A., 102*(42), 15,144–15,148, doi:10.1073/pnas.0505734102.
- Budyko, M. I. (1974), Climate and Life, 508 pp., Academic, New York.
- Buermann, W., B. Parida, M. Jung, G. M. MacDonald, C. J. Tucker, and M. Reichstein (2014), Recent shift in Eurasian boreal forest greening response may be associated with warmer and drier summers, *Geophys. Res. Lett.*, 41, 1995–2002, doi:10.1002/2014GL059450.
- Carpenter, C. (2005), The environmental control of plant species density on a Himalayan elevation gradient, J. Biogeogr., 32(6), 999–1018, doi:10.1111/i.1365-2699.2005.01249.x.
- Christiansen, E., R. H. Waring, and A. A. Berryman (1987), Resistance of conifers to bark beetle attack: Searching for general relationships, For. Ecol. Manage., 22, 89–106.
- Clark, J. S., et al. (2016), The impacts of increasing drought on forest dynamics, structure, and biodiversity in the United States, *Global Change Biol.*, 22, 2329–2352, doi:10.1111/gcb.13160.
- Clow, D. W. (2010), Changes in the timing of snowmelt and streamflow in Colorado: A response to recent warming, *J. Clim.*, 23(9), 2293–2306, doi:10.1175/2009JCLl2951.1.
- Commission for Environmental Cooperation (1997), Ecological Regions of North America: Toward a Common Perspective, Montreal, Que., Canada.
- Cook, R. D. (1979), Influential observations in linear regression, J. Am. Stat. Assoc., 74, 169–174.
- Cornwell, E. N., N. P. Molotch, and J. McPhee (2016), Spatio-temporal variability of snow water equivalent in the extra-tropical Andes Cordillera from distributed energy balance modeling and remotely sensed snow cover, *Hydrol. Earth Syst. Sci.*, 20, 411–430, doi:10.5194/hess-20-411-2016. Davis, M. B., and R. G. Shaw (2001), Range shifts and adaptive responses to Quaternary climate change, *Science*, 292(5517), 673–679, doi:
- 10.1126/science.292.5517.673.

 Dickinson, R. E., A. Henderson-Sellers, and P. J. Kennedy (1993), Biosphere Atmosphere Transfer Scheme (BATS) version 1e as coupled to the NCAR Community Climate Model, NCAR Tech. Note NCAR/TN-387+STR, Natl. Cent. for Atmos. Res., Boulder, Colo.
- Didan, K. (2015), MOD13A3 MODIS/Terra Vegetation Indices Monthly L3 Global 1 km SIN Grid V006, NASA Land Processes Distrib. Active Arch. Cent. (DAAC), doi:10.5067/MODIS/MOD13A3.006.
- Dozier, J. (1989), Spectral signature of alpine snow cover from the Landsat Thematic Mapper, *Remote Sens. Environ.*, 28, 9–22, doi:10.1016/0034-4257(89)90101-6.
- Dozier, J., and J. Frew (1990), Rapid calculation of terrain parameters for radiation modeling from digital elevation data, *IEEE Trans. Geosci. Remote Sens.*, 28(5), 963–969.
- Edburg, S. L., J. A. Hicke, D. M. Lawrence, and P. E. Thornton (2011), Simulating coupled carbon and nitrogen dynamics following mountain pine beetle outbreaks in the western United States, *J. Geophys. Res.*, 116, G04033, doi:10.1029/2011JG001786.
- Edburg, S. L., J. A. Hicke, P. D. Brooks, E. G. Pendall, B. E. Ewers, U. Norton, D. Gochis, E. D. Gutmann, and A. J. Meddens (2012), Cascading impacts of bark beetle-caused tree mortality on coupled biogeophysical and biogeochemical processes, *Frontiers Ecol. Environ.*, 10(8), 416–424, doi:10.1890/10173.
- Emanuel, R. E., H. E. Epstein, B. L. McGlynn, D. L. Welsch, D. J. Muth, and P. D'Odorico (2010), Spatial and temporal controls on watershed ecohydrology in the northern Rocky Mountains, *Water Resour. Res.*, 46, W11553, doi:10.1029/2009WR008890.
- Fettig, C. J., M. L. Reid, B. J. Bentz, S. Sevanto, D. L. Spittlehouse, and T. Wang (2013), Changing climates, changing forests: A western North American perspective, *J. For.*, 111(3), 214–228, doi:10.5849/jof.12-085.
- Gaylord, M. L., T. E. Kolb, W. T. Pockman, J. A. Plaut, E. A. Yepez, A. K. Macalady, R. E. Pangle, and N. G. Mcdowell (2013), Drought predisposes piñon-juniper woodlands to insect attacks and mortality, *New Phytol.*, 198(2), 567–578, doi:10.1111/nph.12174.
- Gitelson, A. A., A. Viña, S. B. Verma, D. C. Rundquist, T. J. Arkebauer, G. Keydan, B. Leavitt, V. Ciganda, G. G. Burba, and A. E. Suyker (2006), Relationship between gross primary production and chlorophyll content in crops: Implications for the synoptic monitoring of vegetation productivity, *J. Geophys. Res.*, 111, D08S11, doi:10.1029/2005JD006017.
- Guan, B., N. P. Molotch, D. E. Waliser, E. J. Fetzer, and P. J. Neiman (2010), Extreme snowfall events linked to atmospheric rivers and surface air temperature via satellite measurements, *Geophys. Res. Lett.*, 37, L20401, doi:10.1029/2010GL044696.
- Guan, B., D. E. Waliser, N. P. Molotch, E. J. Fetzer, and P. J. Neiman (2012), Does the Madden–Julian oscillation influence wintertime atmospheric rivers and snowpack in the Sierra Nevada?, Mon. Weather Rev., 140(2), 325–342, doi:10.1175/MWR-D-11-00087.1.
- Guan, B., N. P. Molotch, D. E. Waliser, S. M. Jepsen, T. H. Painter, and J. Dozier (2013), Snow water equivalent in the Sierra Nevada: Blending snow sensor observations with snowmelt model simulations, *Water Resour. Res.*, 49, 5029–5046, doi:10.1002/wrcr.20387.
- Hall, D. K., and G. A. Riggs (2007), Accuracy assessment of the MODIS snow products, *Hydrol. Processes*, 21(12), 1534–1547, doi:10.1002/hyp.6715.

- Hall, D. K., A. T. C. Chang, and W. M. Kovalick (1990), Satellite-derived reflectance of snow-covered surfaces in northern Minnesota, Remote Sens. Environ., 33(2), 87–96, doi:10.1016/0034-4257(90)90035-K.
- Harpold, A., P. Brooks, S. Rajagopal, I. Heidbuchel, A. Jardine, and C. Stielstra (2012), Changes in snowpack accumulation and ablation in the intermountain west, *Water Resour. Res.*, 48, W11501, doi:10.1029/2012WR011949.
- Hart, S. J., T. T. Veblen, K. S. Eisenhart, D. Jarvis, and D. Kulakowski (2014), Drought induces spruce beetle (*Dendroctonus rufipennis*) outbreaks across northwestern Colorado, *Ecology*, 95(4), 930–939.
- Hicke, J. A., A. J. H. Meddens, C. D. Allen, and C. A. Kolden (2013), Carbon stocks of trees killed by bark beetles and wildfire in the western United States, *Environ. Res. Lett.*, 8(3), 035032, doi:10.1088/1748-9326/8/3/035032.
- Hodges, D. B., G. J. Higgins, P. F. Hilton, R. E. Hood, R. Shapiro, C. N. Touart, and R. F. Wachtmann (1983), Final tactical decision aid (FTDA) for infrared (8–12 micron) systems—Technical background, Rep. AFGL-TR-83–0022, Air Force Geophys. Lab., Hanscom AFB, Mass.
- Homer, C., J. Dewitz, J. Fry, M. Coan, N. Hossain, C. Larson, N. Herold, A. McKerrow, J. N. VanDriel, and J. Wickham (2007), Completion of the 2001 National Land Cover Database for the Coterminous United States, *Photogramm. Eng. Remote Sens.*, 73(4), 337–341.
- Hu, J., D. J. P. Moore, S. P. Burns, and R. K. Monson (2010), Longer growing seasons lead to less carbon sequestration by a subalpine forest, *Global Change Biol.*, 16(2), 771–783, doi:10.1111/j.1365-2486.2009.01967.x.
- Huete, A., K. Didan, T. Miura, E. P. Rodriguez, X. Gao, and L. G. Ferreira (2002), Overview of the radiometric and biophysical performance of the MODIS vegetation indices, *Remote Sens. Environ.*, 83, 195–213.
- Huete, A. R., G. Hua, J. Qi, A. Chehbouni, and W. J. D. van Leeuwen (1992), Normalization of multidirectional red and NIR reflectances with the SAVI, *Remote Sens. Environ.*, 41(2–3), 143–154, doi:10.1016/0034-4257(92)90074-T.
- ldso, S. B. (1981), A set of equations for full spectrum and 8- to 14-μm and 10.5- to 12.5-μm thermal radiation from cloudless skies, *Water Resour. Res.* 17, 295–304
- Jepsen, S. M., N. P. Molotch, M. W. Williams, K. E. Rittger, and J. O. Sickman (2012), Interannual variability of snowmelt in the Sierra Nevada and Rocky Mountains, United States: Examples from two alpine watersheds, Water Resour. Res., 48, W02529, doi:10.1029/2011WR011006.
- Jordan, R. (1991), A one-dimensional temperature model for a snow cover: Technical documentation for SNTHERM.89, *Spec. Rep., 91–16*, 49 pp., U.S. Army Cold Reg. Res. and Eng. Lab., Hanover, N. H.
- Kelsey, R. G., D. Gallego, F. J. Sánchez-García, and J. A. Pajares (2014), Ethanol accumulation during severe drought may signal tree vulnerability to detection and attack by bark beetles, Can. J. For. Res., 44, 554–561, doi:10.1139/cjfr-2013-0428.
- Kirchner, J. W. (2016), Aggregation in environmental systems—Part 1: Seasonal tracer cycles quantify young water fractions, but not mean transit times, in spatially heterogeneous catchments, *Hydrol. Earth Syst. Sci.*, 20, 279–297, doi:10.5194/hess-20-279-2016.
- Knowles, J. F., A. A. Harpold, R. Cowie, M. Zeliff, H. R. Barnard, S. P. Burns, P. D. Blanken, J. F. Morse, and M. W. Williams (2015), The relative contributions of alpine and subalpine systems to the water balance of a mountainous, headwater catchment, *Hydrol. Processes*, 29, 4794–4808, doi:10.1002/hyp.10526.
- Kolb, T. E., C. J. Fettig, M. P. Ayres, B. J. Bentz, J. A. Hicke, R. Mathiasen, J. E. Stewart, and A. S. Weed (2016), Observed and anticipated impacts of drought on forest insects and diseases in the United States, For. Ecol. Manage., 380, 321–334, doi:10.1016/j.foreco.2016.04.051.
- Liston, G. E. (1999), Interrelationships among snow distribution, snowmelt, and snow cover depletion: Implications for atmospheric, hydrologic, and ecologic modeling, *J. Appl. Meteorol.*, 38, 1474–1487.
- Livneh, B., J. S. Deems, B. Buma, J. J. Barsugli, D. Schneider, N. P. Molotch, K. Wolter, and C. A. Wessman (2015), Catchment response to bark beetle outbreak and dust-on-snow in the Colorado Rocky Mountains, J. Hydrol., 523(C), 196–210, doi:10.1016/j.jhydrol.2015.01.039.
- Logan, J. A., W. W. Macfarlane, and L. Willcox (2010), Whitebark pine vulnerability to climate-driven mountain pine beetle disturbance in the Greater Yellowstone Ecosystem, *Ecol. Appl.*, 20(4), 895–902.
- Luce, C. H., J. M. Vose, N. Pederson, J. Campbell, C. Millar, P. Kormos, and R. Woods (2016), Contributing factors for drought in United States forest ecosystems under projected future climates and their uncertainty, For. Ecol. Manage., 380, 299–308, doi:10.1016/j.foreco.2016.05.020.
- Mahrt, L., and M. Ek (1984), The influence of atmospheric stability on potential evaporation, J. Clim. Appl. Meteorol., 23(2), 222–234.
- Maness, H., P. J. Kushner, and I. Fung (2012), Summertime climate response to mountain pine beetle disturbance in British Columbia, *Nat. Geosci.*, 6(1), 65–70, doi:10.1038/ngeo1642.
- Mattson, W. J., and R. A. Haack (1987), The role of drought in outbreaks of plant-eating insects, *BioScience*, *37*(2), 110–118.
- McDowell, N., et al. (2008), Mechanisms of plant survival and mortality during drought: Why do some plants survive while others succumb to drought?, New Phytol., 178, 719–739, doi:10.1111/j.1469-8137.2008.02436.x.
- Meddens, A. J. H., J. A. Hicke, and C. A. Ferguson (2012), Spatiotemporal patterns of observed bark beetle-caused tree mortality in British Columbia and the western United States, *Ecol. Appl.*, 22(7), 1876–1891, doi:10.1890/11-1785.1.
- Meromy, L., N. P. Molotch, T. E. Link, S. R. Fassnacht, and R. Rice (2013), Subgrid variability of snow water equivalent at operational snow stations in the western USA, *Hydrol. Processes*, *27*(17), 2383–2400, doi:10.1002/hyp.9355.
- Mikkelson, K. M., E. R. V. Dickenson, R. M. Maxwell, J. E. McCray, and J. O. Sharp (2013a), Water-quality impacts from climate-induced forest die-off, Nat. Clim. Change, 3(3), 218–222, doi:10.1038/nclimate1724.
- Mikkelson, K. M., L. A. Bearup, R. M. Maxwell, J. D. Stednick, J. E. McCray, and J. O. Sharp (2013b), Bark beetle infestation impacts on nutrient cycling, water quality and interdependent hydrological effects, *Biogeochemistry*, 115(1–3), 1–21, doi:10.1007/s10533-013-9875-8.
- Mitchell, K. E., et al. (2004), The multi-institution North American Land Data Assimilation System (NLDAS): Utilizing multiple GCIP products and partners in a continental distributed hydrological modeling system, *J. Geophys. Res.*, 109, D07S90, doi:10.1029/2003JD003823.
- Molotch, N. P. (2009), Reconstructing snow water equivalent in the Rio Grande headwaters using remotely sensed snow cover data and a spatially distributed snowmelt model, *Hydrol. Processes*, 23(7), 1076–1089, doi:10.1002/hyp.7206.
- Molotch, N. P., and R. C. Bales (2005), Scaling snow observations from the point to the grid element: Implications for observation network design, *Water Resour. Res.*, 41, W11421, doi:10.1029/2005WR004229.
- Molotch, N. P., and R. C. Bales (2006), SNOTEL representativeness in the Rio Grande headwaters on the basis of physiographics and remotely sensed snow cover persistence, *Hydrol. Processes*, 20(4), 723–739, doi:10.1002/hyp.6128.
- Molotch, N. P., and S. A. Margulis (2008), Estimating the distribution of snow water equivalent using remotely sensed snow cover data and a spatially distributed snowmelt model: A multi-resolution, multi-sensor comparison, *Adv. Water Resour.*, 11, 1503–1514, doi:10.1016/i.advwatres.2008.07.017.
- Molotch, N. P., S. R. Fassnacht, R. C. Bales, and S. R. Helfrich (2004), Estimating the distribution of snow water equivalent and snow extent beneath cloud cover in the Salt–Verde River basin, Arizona, *Hydrol. Processes*, 18(9), 1595–1611, doi:10.1002/hyp.1408.
- Molotch, N. P., S. A. Margulis, and S. M. Jepsen (2010), Response to comment by AG Slater, MP Clark, and AP Barrett on 'Estimating the distribution of snow water equivalent using remotely sensed snow cover data and a spatially distributed snowmelt model: A multi-resolution, multi-sensor comparison' [[Adv. Water Resour. 31 (2008) 1503–1514]. Adv. Water Resour., 2009;32(11):1680–4], Adv. Water Resour., 33(2), 231–239, doi:10.1016/j.advwatres.2009.11.008.

- Monson, R. K., A. A. Turnipseed, J. P. Sparks, P. C. Harley, D. Scott, K. L. Sparks, and T. E. Huxman (2002), Carbon sequestration in a high-elevation, subalpine forest, Global Change Biol., 8, 459–478.
- Monson, R. K., J. P. Sparks, T. N. Rosenstiel, L. E. Scott-Denton, T. E. Huxman, P. C. Harley, A. A. Turnipseed, S. P. Burns, B. Backlund, and J. Hu (2005), Climatic influences on net ecosystem CO₂ exchange during the transition from wintertime carbon source to springtime carbon sink in a high-elevation, subalpine forest, *Oecologia*, 146(1), 130–147, doi:10.1007/s00442-005-0169-2.
- Mote, P. W., A. F. Hamlet, M. P. Clark, and D. P. Lettenmaier (2005), Declining mountain snowpack in western North America, Bull. Am. Meteorol. Soc., 86(1), 39–49, doi:10.1175/BAMS-86-1-39.
- Mu, Q. Z., M. S. Zhao, and S. W. Running (2011), Improvements to a MODIS global terrestrial evapotranspiration algorithm, *Remote Sens. Environ.*, 115(8), 1781–1800, doi:10.1016/i.rse.2011.02.019.
- Novick, K. A., et al. (2016), The increasing importance of atmospheric demand for ecosystem water and carbon fluxes, *Nat. Clim. Change*, 6, 1023–1027, doi:10.1038/nclimate3114.
- Painter, T. H., K. Rittger, C. McKenzie, P. Slaughter, R. E. Davis, and J. Dozier (2009), Retrieval of subpixel snow covered area, grain size, and albedo from MODIS, Remote Sens. Environ., 113(4), 868–879, doi:10.1016/j.rse.2009.01.001.
- Pec, G. J., J. Karst, A. N. Sywenky, P. W. Cigan, N. Erbilgin, S. W. Simard, J. F. Cahill Jr. (2015), Rapid increases in forest understory diversity and productivity following a mountain pine beetle (Dendroctonus ponderosae) outbreak in pine forests, *PLoS ONE*, *10*(4), e0124691, doi:10.1371/journal.pone.0124691.
- Peng, S., A. Chen, L. Xu, C. Cao, J. Fang, R. B. Myneni, J. Pinzon, C. J. Tucker, and S. Piao (2011), Recent change of vegetation growth trend in China. Environ. Res. Lett., 6(4), 044027, doi:10.1088/1748-9326/6/4/044027.
- Pepin, N., et al. (2015), Elevation-dependent warming in mountain regions of the world, *Nat. Clim. Change*, 5(5), 424–430, doi:10.1038/nclimate2563.
- Pugh, E., and E. Small (2012), The impact of pine beetle infestation on snow accumulation and melt in the headwaters of the Colorado River, *Ecohydrology*, 5(4), 467–477, doi:10.1002/eco.239.
- Raffa, K. F., B. H. Aukema, N. Erbilgin, K. D. Klepzig, and K. E. Wallin (2005), Interactions among conifer terpenoids and bark beetles across multiple levels of scale: An attempt to understand links between population patterns and physiological processes, *Recent Adv. Phyto-chem.*, 39, 79–118, doi:10.1016/S0079-9920(05)80005-X.
- Reed, D. E., B. E. Ewers, and E. Pendall (2014), Impact of mountain pine beetle induced mortality on forest carbon and water fluxes, *Environ. Res. Lett.*, 9(10), 105004, doi:10.1088/1748-9326/9/10/105004.
- Rice, R., and R. C. Bales (2010), Embedded-sensor network design for snow cover measurements around snow pillow and snow course sites in the Sierra Nevada of California, *Water Resour. Res.*, 46, W03537, doi:10.1029/2008WR007318.
- Rittger, K., T. H. Painter, and J. Dozier (2013), Assessment of methods for mapping snow cover from MODIS, *Adv. Water Resour.*, 51(C), 367–380, doi:10.1016/j.advwatres.2012.03.002.
- Rosenthal, W., and J. Dozier (1996), Automated mapping of montane snow cover at subpixel resolution from the Landsat Thematic Mapper, Water Resour. Res., 32, 115–130.
- Running, S. W., R. R. Nemani, F. A. Heinsch, M. Zhao, M. Reeves, and H. Hashimoto (2004), A continuous satellite-derived measure of global terrestrial primary production, *BioScience*, *54*(6), 547–560.
- Sacks, W. J., D. S. Schimel, and R. K. Monson (2007), Coupling between carbon cycling and climate in a high-elevation, subalpine forest: A model-data fusion analysis, *Oecologia*, 151(1), 54–68, doi:10.1007/s00442-006-0565-2.
- Safranyik, L., A. L. Carroll, J. Régnière, D. W. Langor, W. G. Riel, T. L. Shore, B. Peter, B. J. Cooke, V. G. Nealis, and S. W. Taylor (2010), Potential for range expansion of mountain pine beetle into the boreal forest of North America, Can. Entomol., 142(5), 415–442, doi:10.4039/n08-CPA01.
- Schimel, D. S., T. G. F. Kittel, S. Running, R. Monson, A. Turnipseed, and D. Anderson (2002), Carbon sequestration studied in western U.S. mountains, Eos Trans. AGU, 83(40), 445, doi:10.1029/2002E0000314.
- Schneider, D., and N. P. Molotch (2016), Real-time estimation of snow water equivalent in the Upper Colorado River Basin using MODIS-based SWE reconstructions and SNOTEL data, *Water Resour. Res.*, 52, 7892–7910, doi:10.1002/2016WR019067.
- Slater, A. G., A. P. Barrett, M. P. Clark, J. D. Lundquist, and M. S. Raleigh (2013), Uncertainty in seasonal snow reconstruction: Relative impacts of model forcing and image availability, *Adv. Water Resour.*, 55(C), 165–177, doi:10.1016/j.advwatres.2012.07.006.
- Stewart, I. T., D. R. Cayan, and M. D. Dettinger (2005), Changes toward earlier streamflow timing across western North America, *J. Clim.*, 18, 1136–1155.
- Stinziano, J. R., and D. A. Way (2014), Combined effects of rising [CO₂] and temperature on boreal forests: Growth, physiology and limitations, Botany, 92(6), 425–436, doi:10.1139/cjb-2013-0314.
- Sun, S.-L., G. Sun, P. Caldwell, S. McNulty, E. Cohen, J.-F. Xiao, and Y. Zhang (2015), Drought impacts on ecosystem functions of the U.S. National Forests and Grasslands: Part 1. Evaluation of a water and carbon balance model, For. Ecol. Manage., 353, 260–268, doi:10.1016/i.foreco.2015.03.054.
- Trujillo, E., and N. P. Molotch (2014), Snowpack regimes of the Western United States, *Water Resour. Res.*, 50, 5611–5623, doi:10.1002/2013WR014753.
- Trujillo, E., N. P. Molotch, M. L. Goulden, A. E. Kelly, and R. C. Bales (2012), Elevation-dependent influence of snow accumulation on forest greening, *Nat. Geosci.*, 5(10), 705–709, doi:10.1038/ngeo1571.
- United States Environmental Protection Agency (2010), Level III Ecoregions of the Continental United States, U.S. EPA National Health and Environmental Effects Research Laboratory, Map M-1, Various Scales, Corvallis, Oreg.
- Vose, J. M., C. F. Miniat, C. H. Luce, H. Asbjornsen, P. V. Caldwell, J. L. Campbell, G. E. Grant, D. J. Isaak, S. P. Loheide II, and G. Sun (2016), Ecohydrological implications of drought for forests in the United States, For. Ecol. Manage., 380, 335–345, doi:10.1016/j.foreco.2016.03.025.
- Westerling, A. L., H. G. Hidalgo, D. R. Cayan, and T. W. Swetnam (2006), Warming and earlier spring increase western U.S. forest wildfire activity, *Science*, 313(5789), 940–943, doi:10.1126/science.1128834.
- Winchell, T. S., D. M. Barnard, R. K. Monson, S. P. Burns, and N. P. Molotch (2016), Earlier snowmelt reduces atmospheric carbon uptake in midlatitude subalpine forests, Geophys. Res. Lett., 43, 8160–8168, doi:10.1002/2016GL069769.
- Wu, X., H. Liu, D. Guo, O. A. Anenkhonov, N. K. Badmaeva, and D. V. Sandanov (2012), Growth decline linked to warming-induced water limitation in hemi-boreal forests, *PLoS ONE*, 7(8), e42619, doi:10.1371/journal.pone.0042619.s003.
- Xia, Y., et al. (2012), Continental-scale water and energy flux analysis and validation for the North American Land Data Assimilation System project phase 2 (NLDAS-2): 1. Intercomparison and application of model products, *J. Geophys. Res., 117*, D03109, doi:10.1029/2011JD016048.
- Zhao, M., F. A. Heinsch, R. R. Nemani, and S. W. Running (2005), Improvements of the MODIS terrestrial gross and net primary production global data set, *Remote Sens. Environ.*, 95(2), 164–176, doi:10.1016/j.rse.2004.12.011.